Journal of Computational Physics 231 (2012) 2510–2527

Contents lists available at SciVerse ScienceDirect

Journal of Computational Physics

journal homepage: www.elsevier.com/locate/jcp

Efficient implementation of high order inverse Lax–Wendroff boundary treatment for conservation laws

Sirui Tan [a], Cheng Wang [b,*], Chi-Wang Shu [a], Jianguo Ning [b]

[a] Division of Applied Mathematics, Brown University, Providence, RI 02912, United States
[b] State Key Laboratory of Explosion Science and Technology, Beijing Institute of Technology, Beijing 100081, PR China

ARTICLE INFO

Article history:
Received 14 July 2011
Received in revised form 21 October 2011
Accepted 29 November 2011
Available online 9 December 2011

Keywords:
Numerical boundary conditions
Hyperbolic conservation laws
Cartesian mesh
Inverse Lax–Wendroff procedure
Reactive Euler equations
Detonation
No-penetration conditions

ABSTRACT

In [20], two of the authors developed a high order accurate numerical boundary condition procedure for hyperbolic conservation laws, which allows the computation using high order finite difference schemes on Cartesian meshes to solve problems in arbitrary physical domains whose boundaries do not coincide with grid lines. This procedure is based on the so-called inverse Lax–Wendroff (ILW) procedure for inflow boundary conditions and high order extrapolation for outflow boundary conditions. However, the algebra of the ILW procedure is quite heavy for two dimensional (2D) hyperbolic systems, which makes it difficult to implement the procedure for order of accuracy higher than three. In this paper, we first discuss a simplified and improved implementation for this procedure, which uses the relatively complicated ILW procedure only for the evaluation of the first order normal derivatives. Fifth order WENO type extrapolation is used for all other derivatives, regardless of the direction of the local characteristics and the smoothness of the solution. This makes the implementation of a fifth order boundary treatment practical for 2D systems with source terms. For no-penetration boundary condition of compressible inviscid flows, a further simplification is discussed, in which the evaluation of the tangential derivatives involved in the ILW procedure is avoided. We test our simplified and improved boundary treatment for Euler equations with or without source terms representing chemical reactions in detonations. The results demonstrate the designed fifth order accuracy, stability, and good performance for problems involving complicated interactions between detonation/shock waves and solid boundaries.

1. Introduction

In [20], two of the authors developed a high order accurate numerical boundary condition procedure for finite difference methods for solving hyperbolic conservation laws on a Cartesian mesh, while the physical domain can be arbitrarily shaped. The challenge is that the physical boundary does not usually coincide with grid lines and can intersect the Cartesian grids in an arbitrary fashion. For the sake of accuracy and stability, a so-called inverse Lax–Wendroff (ILW) procedure was developed. This procedure was first proposed by Goldberg and Tadmor [6,7] for analyzing numerical boundary conditions of linear hyperbolic equations in one dimension with boundaries aligned with grid lines. It helps us obtain normal derivatives at inflow boundaries from time derivatives and tangential derivatives by a repeated use of the partial differential equations (PDEs). Together with high order extrapolation at outflow boundaries, we can impose accurate values of the ghost points near the boundaries by a Taylor expansion. Numerical examples in [20] show that this method is high order accurate and

* Corresponding author. Tel.: +86 10 68914456; fax: +86 10 68911040.
E-mail addresses: sirui@dam.brown.edu (S. Tan), wangcheng@bit.edu.cn (C. Wang), shu@dam.brown.edu (C.-W. Shu), jgning@bit.edu.cn (J. Ning).

0021-9991/$ - see front matter © 2011 Elsevier Inc. All rights reserved.
doi:10.1016/j.jcp.2011.11.037

stable under the standard CFL conditions determined by the interior schemes. In [21], this approach was extended to solve compressible inviscid flows involving complex moving geometries.

The algebra of the ILW procedure, which relies on the PDEs, can be very heavy for fully nonlinear systems of equations in two dimensions (2D). Of course, it would be even heavier for 2D problems with source terms. For this reason, in [20,21] we only implemented third order boundary treatment for 2D Euler equations, although our method was designed to achieve arbitrarily high order accuracy for general equations with source terms.

In this paper, we aim to simplify and improve our boundary treatment procedure such that it is easier to implement for achieving higher order accuracy. We demonstrate this simplified and efficient procedure on the scheme with fifth order accuracy, which is the same order as our interior scheme, for both 2D regular Euler equations and 2D reactive Euler equations which contain source terms representing one-step chemical reactions in detonations. We investigate each term in the Taylor expansion and find that only the first two terms, i.e., the constant term and the first order normal derivative term, are crucial to be implemented by the costly ILW procedure to ensure stability. In other words, near the inflow boundaries, only the first order normal derivative needs to be obtained by the ILW procedure. All the higher order normal derivatives can simply be obtained by extrapolation of a suitable order. This simplified algorithm significantly alleviates the complicated algebra in the ILW procedure, especially for 2D systems with source terms. We note that a similar idea was proposed by Qiu and Shu for the Lax–Wendroff time discretization [15], in which they performed a weighted essentially non-oscillatory (WENO) approximation only for the reconstruction of the fluxes to the first order time derivative to avoid spurious oscillations and used the inexpensive central difference approximation for the reconstruction of the higher order time derivatives.

The ILW procedure can be further simplified for no-penetration boundary condition at solid walls of compressible inviscid flows with or without chemical reactions. In this special but important case, the first order time derivative of the normal momentum can be converted to the first order normal derivatives without introducing any tangential derivatives. As a result, we do not need to do any numerical differentiation. The same conclusion can be made if we consider (reactive) Euler equations in primitive variables. In fact, the effectiveness and robustness of imposing primitive variables instead of conservative variables was verified in [21] where the no-penetration boundary condition is prescribed in normal velocity.

Our fifth order boundary treatment requires fifth order extrapolation for both smooth solutions and solutions containing strong discontinuities. In [20], we used Lagrange extrapolation or least squares extrapolation if the solution is smooth near the boundary. Otherwise, we developed a third order accurate WENO type extrapolation to prevent overshoot or undershoot near the discontinuities. We extend the WENO type extrapolation to fifth order accuracy in this paper and use it in both smooth and non-smooth cases. In this sense, our method is improved to be more uniform.

There are many successful boundary treatment techniques based on Cartesian grids besides [20]. Unfortunately, most of them are at most second order accurate. For example, a Cartesian embedded boundary method was developed to solve the wave equation with Dirichlet or Neumann boundary conditions in [10–12] and to solve hyperbolic conservation laws in [19]. An internal boundary method based on a reflection technique and interpolation was developed to solve ideal and non-ideal compressible reactive flows in [27] and detonation problems in [13,23,24]. Engineering applications in detonations usually require simulations be carried out for complex geometries. This involves interaction of detonations with complex solid boundaries. If the accuracy of numerical boundary treatment is low, the error will pollute the computational results in internal domain although the computational accuracy of internal domain is of high order. Thus, it is necessary to construct a high order numerical boundary treatment to investigate complicated interactions between detonations and solid boundaries.

The remainder of the paper is organized as follows. We first give an overview of the discretization of the problem. Then we concentrate on the issue of imposing the values of ghost points. For 1D Euler equations, we propose that the kth order spatial derivatives, $k \geqslant 2$, can simply be obtained by extrapolation in all circumstances. The fifth order WENO type extrapolation is developed for this purpose. The improvement for 1D problems is extended to 2D reactive Euler equations. The tangential derivatives in the 2D ILW procedure can be avoided in the case of no-penetration boundary condition at solid walls. Numerical examples of (reactive) Euler equations are shown in Section 3. We can see our boundary treatment is fifth order accurate, stable, and capable of treating interactions between denotation/shock waves and solid boundaries with good resolution. Concluding remarks are given in Section 4.

2. Scheme formulation

We consider strongly hyperbolic conservation laws possibly with source term for $\boldsymbol{U} = \boldsymbol{U}(x,y,t) \in \mathbb{R}^2$

$$\begin{cases} \boldsymbol{U}_t + \boldsymbol{F}(\boldsymbol{U})_x + \boldsymbol{G}(\boldsymbol{U})_y = \boldsymbol{S}(\boldsymbol{U}) & (x,y) \in \Omega, \quad t > 0, \\ \boldsymbol{U}(x,y,0) = \boldsymbol{U}_0(x,y) & (x,y) \in \overline{\Omega}, \end{cases} \tag{2.1}$$

on a bounded domain Ω with appropriate boundary conditions prescribed on $\partial\Omega$ at time t. We assume Ω is covered by a uniform Cartesian mesh with mesh size $\Delta x = \Delta y = h$, but the boundary $\partial\Omega$ does not need to coincide with any grid lines. The semi-discrete approximation of (2.1) is given by

$$\frac{d}{dt}\boldsymbol{U}_{ij}(t) = -\frac{1}{h}\left(\widehat{\boldsymbol{F}}_{i+1/2,j} - \widehat{\boldsymbol{F}}_{i-1/2,j}\right) - \frac{1}{h}\left(\widehat{\boldsymbol{G}}_{ij+1/2} - \widehat{\boldsymbol{G}}_{ij-1/2}\right) + \boldsymbol{S}(\boldsymbol{U}_{ij}(t)), \tag{2.2}$$

where $\widehat{\boldsymbol{F}}_{i+1/2,j}$ and $\widehat{\boldsymbol{G}}_{i,j+1/2}$ are the numerical fluxes. We use a third order total variation diminishing Runge–Kutta (RK) method [18] to integrate the system of ordinary differential equations (2.2) in time

$$\begin{aligned}
\boldsymbol{U}_{i,j}^{(1)} &= \boldsymbol{U}_{i,j}^{n} + \Delta t\mathcal{L}\left(\boldsymbol{U}_{i,j}^{n}\right),\\
\boldsymbol{U}_{i,j}^{(2)} &= \frac{3}{4}\boldsymbol{U}_{i,j}^{n} + \frac{1}{4}\boldsymbol{U}_{i,j}^{(1)} + \frac{1}{4}\Delta t\mathcal{L}\left(\boldsymbol{U}_{i,j}^{(1)}\right),\\
\boldsymbol{U}_{i,j}^{n+1} &= \frac{1}{3}\boldsymbol{U}_{i,j}^{n} + \frac{2}{3}\boldsymbol{U}_{i,j}^{(2)} + \frac{2}{3}\Delta t\mathcal{L}\left(\boldsymbol{U}_{i,j}^{(2)}\right),
\end{aligned} \tag{2.3}$$

where $\mathcal{L}(\cdot)$ is the operator defined by the right-hand side of (2.2).

Suppose we have a time dependent boundary condition $\boldsymbol{g}(t)$. Following the idea in [3], we can easily show that for the hyperbolic system (2.1) with source term the following match of time levels at the boundary maintains the third order accuracy of (2.3)

$$\begin{aligned}
\boldsymbol{U}^{n} &\sim \boldsymbol{g}(t_n),\\
\boldsymbol{U}^{(1)} &\sim \boldsymbol{g}(t_n) + \Delta t\boldsymbol{g}'(t_n),\\
\boldsymbol{U}^{(2)} &\sim \boldsymbol{g}(t_n) + \frac{1}{2}\Delta t\boldsymbol{g}'(t_n) + \frac{1}{4}\Delta t^2\boldsymbol{g}''(t_n).
\end{aligned} \tag{2.4}$$

For simplicity, we denote the boundary conditions for all three stages at time level $t = t_n$ by $\boldsymbol{g}(t_n)$, although $\boldsymbol{g}(t_n)$ is actually different for each stage according to (2.4).

We use the fifth order finite difference WENO scheme with the Lax–Friedrichs flux splitting [9] to form the numerical fluxes $\widehat{\boldsymbol{F}}_{i+1/2,j}$ and $\widehat{\boldsymbol{G}}_{i,j+1/2}$ in (2.2). The scheme requires a seven point stencil in both x and y directions. Near $\partial\Omega$ where the numerical stencil is partially outside of Ω, up to three ghost points are needed in each direction. We concentrate on how to define the values of the ghost points at time level $t = t_n$ in the rest of the paper.

2.1. One-dimensional systems

We consider 1D compressible Euler equations without source term

$$\boldsymbol{U}_t + \boldsymbol{F}(\boldsymbol{U})_x = 0, \quad x \in (-1,1), \quad t > 0,$$

where the conservative variables

$$\boldsymbol{U} = \begin{pmatrix} U_1 \\ U_2 \\ U_3 \end{pmatrix} = \begin{pmatrix} \rho \\ \rho u \\ E \end{pmatrix}$$

and the flux

$$\boldsymbol{F}(\boldsymbol{U}) = \begin{pmatrix} U_2 \\ (\gamma-1)U_3 + \frac{3-\gamma}{2}\frac{U_2^2}{U_1} \\ \left(\gamma U_3 - \frac{\gamma-1}{2}\frac{U_2^2}{U_1}\right)\frac{U_2}{U_1} \end{pmatrix} = \begin{pmatrix} \rho u \\ \rho u^2 + p \\ u(E+p) \end{pmatrix}.$$

ρ, u, p and E describe the density, velocity, pressure and total energy, respectively. The equation of state has the form

$$E = \frac{p}{\gamma-1} + \frac{1}{2}\rho u^2,$$

where γ is the (constant) specific heat ratio. The sound speed is $c = \sqrt{\gamma p/\rho}$. We consider the right boundary $x = 1$. The left boundary can be treated similarly.

Let us discretize the interval $(-1,1)$ by a uniform mesh

$$-1 + h/2 = x_0 < x_1 < \cdots < x_N = 1 - h/2.$$

We assume $\boldsymbol{U}_0,\ldots,\boldsymbol{U}_N$ have been updated from time level t_{n-1} to time level t_n. Here we suppress the t_n dependence without causing any confusion. We proceed as in [20] to construct values of ghost points $\boldsymbol{U}_{N+1},\ldots,\boldsymbol{U}_{N+3}$ by a fourth order Taylor expansion

$$(U_m)_j = \sum_{k=0}^{4} \frac{(x_j-1)^k}{k!} U_m^{*(k)}, \quad m = 1,2,3, \quad j = N+1,\ldots,N+3, \tag{2.5}$$

where $U_m^{*(k)}$ is a $(5-k)$th order approximation of the spatial derivative $\left.\frac{\partial^k U_m}{\partial x^k}\right|_{x=1,t=t_n}$.

We first do a local characteristic decomposition to decide the inflow and outflow boundary conditions. Denote the Jacobian matrix of the flux near the boundary by

$$\boldsymbol{A}_\perp(\boldsymbol{U}_N) = \left.\frac{\partial \boldsymbol{F}(\boldsymbol{U})}{\partial \boldsymbol{U}}\right|_{\boldsymbol{U}=\boldsymbol{U}_N}.$$

$\boldsymbol{A}_\perp(\boldsymbol{U}_N)$ has three eigenvalues $\lambda_1 = u_N - c_N$, $\lambda_2 = u_N$, $\lambda_3 = u_N + c_N$ and a complete set of left eigenvectors $\boldsymbol{l}_1(\boldsymbol{U}_N)$, $\boldsymbol{l}_2(\boldsymbol{U}_N)$, $\boldsymbol{l}_3(\boldsymbol{U}_N)$ which forms a matrix

$$\boldsymbol{L}(\boldsymbol{U}_N) = \begin{pmatrix} \boldsymbol{l}_1(\boldsymbol{U}_N) \\ \boldsymbol{l}_2(\boldsymbol{U}_N) \\ \boldsymbol{l}_3(\boldsymbol{U}_N) \end{pmatrix} = \begin{pmatrix} l_{1,1} & l_{1,2} & l_{1,3} \\ l_{2,1} & l_{2,2} & l_{2,3} \\ l_{3,1} & l_{3,2} & l_{3,3} \end{pmatrix}.$$

For definiteness, we assume $\lambda_1 < \lambda_2 < 0$ and $\lambda_3 > 0$. Thus two boundary conditions are needed, for example, $U_m(1,t) = g_m(t)$, $m = 1,2$. We define the local characteristic variables V_m at grid points near the boundary by

$$(V_m)_j = \boldsymbol{l}_m(\boldsymbol{U}_N)\boldsymbol{U}_j, \quad m = 1,2,3, \quad j = N-4,\ldots,N. \tag{2.6}$$

We extrapolate $(V_m)_j$ to the boundary with a fifth order WENO type extrapolation and denote the extrapolated kth order derivative of V_m at the boundary by $V_m^{*(k)},\ k = 0,\ldots,4,\ m = 1,2,3$. The WENO type extrapolation will be described in detail in the next subsection.

We impose $U_1^{*(0)} = g_1(t_n)$ and $U_2^{*(0)} = g_2(t_n)$. Because of the signs of the corresponding eigenvalues, V_1, V_2 are the ingoing local characteristic variables and V_3 is outgoing. Therefore, for stability reason, $U_3^{*(0)}$ is solved by the extrapolation equation of V_3

$$l_{3,1}U_1^{*(0)} + l_{3,2}U_2^{*(0)} + l_{3,3}U_3^{*(0)} = V_3^{*(0)}. \tag{2.7}$$

Notice that the coefficient $l_{3,3} = \frac{\gamma-1}{2c_N^2}$ never vanishes. Next we find the first spatial derivatives $U_m^{*(1)}$ with the ILW procedure for U_1 and U_2, together with the extrapolation equation of V_3. Using the first two equations of the Euler system, we write the first time derivatives of U_1,U_2 as

$$\begin{aligned} &\frac{\partial U_1}{\partial t} = -\frac{\partial U_2}{\partial x}, \\ &\frac{\partial U_2}{\partial t} = -(\gamma-1)\frac{\partial U_3}{\partial x} - \frac{3-\gamma}{2}\left(\frac{2U_2}{U_1}\frac{\partial U_2}{\partial x} - \frac{U_2^2}{U_1^2}\frac{\partial U_1}{\partial x}\right). \end{aligned}$$

Notice that the left-hand side of the above equations is already known at the boundary. $U_m^{*(1)}$ can then be solved by the linear system

$$\begin{aligned} &U_2^{*(1)} = -g_1'(t_n), \\ &(\gamma-1)U_3^{*(1)} + \frac{3-\gamma}{2}\left[\frac{2U_2^{*(0)}}{U_1^{*(0)}}U_2^{*(1)} - \left(\frac{U_2^{*(0)}}{U_1^{*(0)}}\right)^2 U_1^{*(1)}\right] = -g_2'(t_n), \\ &l_{3,1}U_1^{*(1)} + l_{3,2}U_2^{*(1)} + l_{3,3}U_3^{*(1)} = V_3^{*(1)}. \end{aligned} \tag{2.8}$$

Repeatedly using the Euler equations and the extrapolation equation, we are able to solve $U_m^{*(k)},\ k = 2,3,4$. However, the algebra of the ILW procedure becomes more and more complicated for larger k. See [20] for the formulas of $k = 2$. In fact, the scheme is still stable if we simply obtain $U_m^{*(k)},\ k = 2,3,4$, by extrapolation. Namely,

$$\boldsymbol{L}(\boldsymbol{U}_N)\begin{pmatrix} U_1^{*(k)} \\ U_2^{*(k)} \\ U_3^{*(k)} \end{pmatrix} = \begin{pmatrix} V_1^{*(k)} \\ V_2^{*(k)} \\ V_3^{*(k)} \end{pmatrix}. \tag{2.9}$$

In other words, the complicated ILW procedure is not needed for spatial derivatives of order higher than or equal to two, regardless of the direction of the local characteristic variables. We remark that instability is observed in our numerical experiments if the first order spatial derivatives are also obtained by extrapolation. Therefore, the ILW procedure is crucial to ensure stability.

We summarize our fifth order boundary treatment at the right boundary $x = 1$ as follows, assuming that $\boldsymbol{U}_j$, $j = 0,\ldots,N$, have been updated from time level t_{n-1} to time level t_n.

1. Compute the eigenvalues $\lambda_m(\boldsymbol{U}_N)$ and left eigenvectors $\boldsymbol{l}_m(\boldsymbol{U}_N)$ of the Jacobian matrix $\boldsymbol{A}_\perp(\boldsymbol{U}_N)$ for $m = 1,2,3$. Decide the prescribed inflow boundary conditions $g_m(t)$ according to the signs of $\lambda_m(\boldsymbol{U}_N)$.
2. Form the local characteristic variables $(V_m)_j$, $j = N-4,\ldots,N$, as in (2.6). Obtain $V_m^{*(k)}$, which is a $(5-k)$th order approximation of the kth order derivative of V_m at the boundary, by the WENO type extrapolation. See the next subsection for details.
3. Solve for $U_m^{*(0)},\ m = 1,2,3$, by the prescribed boundary conditions and extrapolated values $V_m^{*(0)}$, such as (2.7).

4. Use the ILW procedure to write the first derivative of $g_m(t)$ as a linear combination of first spatial derivatives. Together with the extrapolation equations, form a linear system with $U_m^{*(1)}$ as unknowns, such as (2.8). Solve for $U_m^{*(1)},\ m = 1,2,3$.
5. For $k = 2,3,4$, solve for $U_m^{*(k)}$ by extrapolation Eq. (2.9). The ILW procedure is not needed in this step.
6. Impose the values of ghost points by the Taylor expansion (2.5).

For the case of no-penetration boundary condition at solid walls, i.e., $u = 0$, the second eigenvalue of the Jacobian matrix $\boldsymbol{A}_\perp(\boldsymbol{U}_N)$ is approximately zero. In this situation, the direction of the local characteristic variable V_2 is not clear. We will discuss this issue for 2D problems in Section 2.3. We finally remark that we use fifth order WENO type extrapolation in Step 2 regardless of the smoothness of the solution.

2.2. 1D WENO type extrapolation

We need to obtain a $(5-k)$th order approximation of the kth order derivative of the local characteristic variables V_m at the boundary, using the grid point values in the interior of the domain $(V_m)_j, j = N-4,\ldots,N$. See Step 2 of the algorithm flowchart in Section 2.1. For the ease of notation, we suppress the subscript of V in this subsection since each component is extrapolated by the same method.

If V is smooth near the boundary, the extrapolation can be easily done by constructing a Lagrange polynomial $p_4(x)$ interpolating V_j, $j = N-4,\ldots,N$, and evaluating the kth order derivative of $p_4(x)$ at the boundary. However, if a discontinuity appears in the stencil $S_4 = \{x_{N-4},\ldots,x_N\}$, Lagrange extrapolation may lead to severe overshoot or undershoot near the discontinuity. In this situation, we prefer a lower order accurate but more robust extrapolation. A third order accurate WENO type extrapolation was developed in Section 2.2 of [20]. We extend it to fifth order accuracy here.

We consider the stencil S_4 as five candidate substencils $S_r = \{x_{N-r},\ldots,x_N\}$, $r = 0,\ldots,4$. On each substencil, we can easily construct a Lagrange polynomial $p_r(x)$ of degree r such that $p_r(x_j) = V_j$, $j = N-r,\ldots,N$. Suppose V is smooth on S_4, $V^{*(k)}$ can be extrapolated by

$$V^{*(k)} = \sum_{r=0}^{4} d_r \left.\frac{d^k p_r(x)}{dx^k}\right|_{x=1},$$

where $d_0 = h^4,\ d_1 = h^3,\ d_2 = h^2,\ d_3 = h,\ d_4 = 1 - \sum_{r=0}^{3} d_r$.

We look for WENO type extrapolation in the form

$$V^{*(k)} = \sum_{r=0}^{4} \omega_r \left.\frac{d^k p_r(x)}{dx^k}\right|_{x=1}, \tag{2.10}$$

where ω_r are the nonlinear weights depending on the value of V_j. In the case that V is smooth in S_4, we would like to have

$$\omega_0 = O(h^4), \quad \omega_1 = O(h^3), \quad \omega_2 = O(h^2), \omega_3 = O(h) \quad \text{and} \quad \omega_4 = 1 - \sum_{r=0}^{3} \omega_r \tag{2.11}$$

such that (2.10) is $(5-k)$th order accurate. The nonlinear weights ω_r are defined by

$$\omega_r = \frac{\alpha_r}{\sum_{s=0}^{4} \alpha_s}$$

with

$$\alpha_r = \frac{d_r}{(\varepsilon + \beta_r)^q}, \tag{2.12}$$

where $\varepsilon = 10^{-6}$, $q \geqslant 3$ is an integer and β_r are the smoothness indicators determined by

$$\beta_0 = h^2,$$
$$\beta_r = \sum_{l=1}^{r} \int_1^{1+h} h^{2l-1} \left(\frac{d^l}{dx^l} p_r(x)\right)^2 dx, \quad r = 1,\ldots,4.$$

The explicit expressions for the smoothness indicators β_1 and β_2 can be found in Eqs. (2.15) and (2.16) in [20]. The expressions for β_3 and β_4 are tedious but can be easily derived by symbolic computation softwares.

We can show that (2.11) holds if V is smooth in S_4. If S_r, $r \geqslant 1$, contains a discontinuity but S_{r-1} does not, we have $\omega_s = O(h^{r-1-s})$, $s = 0,\ldots,r-1$, and $\omega_s = O(h^{2q+r-1-s})$, $s = r,\ldots,4$. Namely, $V^{*(0)}$ reduces to a rth order approximation and as $h \to 0$ the weights assigned to the non-smooth substencils $S_r,\ldots,S_4$ vanish. The proof is similar to that in Section 2.2 of [20] and is omitted here.

2.3. Two-dimensional problems

We consider 2D compressible reactive Euler equations

$$\boldsymbol{U}_t + \boldsymbol{F}(\boldsymbol{U})_x + \boldsymbol{G}(\boldsymbol{U})_y = \boldsymbol{S}(\boldsymbol{U}), \quad (x,y) \in \Omega, \quad t > 0, \tag{2.13}$$

where

$$\boldsymbol{U} = \begin{pmatrix} U_1 \\ U_2 \\ U_3 \\ U_4 \\ U_5 \end{pmatrix} = \begin{pmatrix} \rho \\ \rho u \\ \rho v \\ E \\ \rho Y \end{pmatrix}, \quad \boldsymbol{F}(\boldsymbol{U}) = \begin{pmatrix} \rho u \\ \rho u^2 + p \\ \rho u v \\ u(E+p) \\ \rho u Y \end{pmatrix},$$

$$\boldsymbol{G}(\boldsymbol{U}) = \begin{pmatrix} \rho v \\ \rho u v \\ \rho v^2 + p \\ v(E+p) \\ \rho v Y \end{pmatrix}, \quad \boldsymbol{S}(\boldsymbol{U}) = \begin{pmatrix} 0 \\ 0 \\ 0 \\ 0 \\ \omega \end{pmatrix}.$$

Y describes the reactant mass fraction and the source term is assumed to be in an Arrhenius form

$$\omega = -K_c \rho Y e^{-T^+/T},$$

where $T = p/\rho$ is the temperature, T^+ is the activation temperature and K_c is a constant. The equation of state has the form

$$E = \frac{p}{\gamma - 1} + \frac{1}{2}\rho(u^2 + v^2) + \rho Q Y, \tag{2.14}$$

where Q is the (constant) heat release due to the chemical reaction. Notice that if $Y \equiv 0$, then (2.13) reduces to the usual compressible Euler equations without source term.

We proceed as in Section 2.5 of [20]. We assume the values of all the grid points inside Ω have been updated from time level t_{n-1} to time level t_n. For a ghost point $P = (x_i, y_j)$, we find a point $P_0 = (x_0, y_0) = \boldsymbol{x}_0$ on the boundary $\partial\Omega$ such that the normal $\boldsymbol{n}(\boldsymbol{x}_0)$ at P_0 goes through P. The sign of the normal $\boldsymbol{n}(\boldsymbol{x}_0)$ is chosen in such a way that it is positive if it points to the exterior of Ω. We set up a local coordinate system at P_0 by

$$\begin{pmatrix} \hat{x} \\ \hat{y} \end{pmatrix} = \begin{pmatrix} \cos\theta & \sin\theta \\ -\sin\theta & \cos\theta \end{pmatrix} \begin{pmatrix} x \\ y \end{pmatrix} = \boldsymbol{T} \begin{pmatrix} x \\ y \end{pmatrix}, \tag{2.15}$$

where θ is the angle between the normal $\boldsymbol{n}(\boldsymbol{x}_0)$ and the x-axis and $\boldsymbol{T}$ is a rotational matrix. The $\hat{x}$-axis then points in the same direction as $\boldsymbol{n}(\boldsymbol{x}_0)$ and the $\hat{y}$-axis points in the tangential direction. In this local coordinate system, the reactive Euler equations (2.13) are written as

$$\widehat{\boldsymbol{U}}_t + \boldsymbol{F}\left(\widehat{\boldsymbol{U}}\right)_{\hat{x}} + \boldsymbol{G}\left(\widehat{\boldsymbol{U}}\right)_{\hat{y}} = \boldsymbol{S}\left(\widehat{\boldsymbol{U}}\right), \tag{2.16}$$

where

$$\widehat{\boldsymbol{U}} = \begin{pmatrix} \widehat{U}_1 \\ \widehat{U}_2 \\ \widehat{U}_3 \\ \widehat{U}_4 \\ \widehat{U}_5 \end{pmatrix} = \begin{pmatrix} \rho \\ \rho\hat{u} \\ \rho\hat{v} \\ E \\ \rho Y \end{pmatrix}, \quad \begin{pmatrix} \hat{u} \\ \hat{v} \end{pmatrix} = \boldsymbol{T} \begin{pmatrix} u \\ v \end{pmatrix}.$$

For a fifth order boundary treatment, the value of the ghost point P is imposed by the Taylor expansion

$$\left(\widehat{U}_m\right)_{i,j} = \sum_{k=0}^{4} \frac{\Delta^k}{k!} \widehat{U}_m^{*(k)}, \quad m = 1, \ldots, 5, \tag{2.17}$$

where Δ is the $\hat{x}$-coordinate of P and $\widehat{U}_m^{*(k)}$ is a $(5-k)$th order approximation of the normal derivative $\left.\frac{\partial^k \widehat{U}_m}{\partial \hat{x}^k}\right|_{(x,y)=\boldsymbol{x}_0, t=t_n}$. We assume $\hat{\boldsymbol{U}}_0$ is the value of a grid point nearest to P_0 among all the grid points inside Ω. We denote the Jacobian matrix of the normal flux by

$$\boldsymbol{A}_\perp\left(\widehat{\boldsymbol{U}}_0\right)=\left.\frac{\partial \boldsymbol{F}\left(\widehat{\boldsymbol{U}}\right)}{\partial \widehat{\boldsymbol{U}}}\right|_{\widehat{\boldsymbol{U}}=\widehat{\boldsymbol{U}}_0}.$$

$\boldsymbol{A}_\perp\left(\widehat{\boldsymbol{U}}_0\right)$ has five eigenvalues $\lambda_1=\hat{u}_0-c_0,\ \lambda_2=\lambda_3=\lambda_4=\hat{u}_0,\ \lambda_5=\hat{u}_0+c_0$ and a complete set of left eigenvectors $\boldsymbol{l}_m\left(\widehat{\boldsymbol{U}}_0\right),\ m=1,\dots,5$, which forms a matrix

$$\boldsymbol{L}\left(\widehat{\boldsymbol{U}}_0\right)=\begin{pmatrix}\boldsymbol{l}_1\left(\widehat{\boldsymbol{U}}_0\right)\\ \boldsymbol{l}_2\left(\widehat{\boldsymbol{U}}_0\right)\\ \boldsymbol{l}_3\left(\widehat{\boldsymbol{U}}_0\right)\\ \boldsymbol{l}_4\left(\widehat{\boldsymbol{U}}_0\right)\\ \boldsymbol{l}_5\left(\widehat{\boldsymbol{U}}_0\right)\end{pmatrix}=\begin{pmatrix}l_{1,1}&l_{1,2}&l_{1,3}&l_{1,4}&l_{1,5}\\ l_{2,1}&l_{2,2}&l_{2,3}&l_{2,4}&l_{2,5}\\ l_{3,1}&l_{3,2}&l_{3,3}&l_{3,4}&l_{3,5}\\ l_{4,1}&l_{4,2}&l_{4,3}&l_{4,4}&l_{4,5}\\ l_{5,1}&l_{5,2}&l_{5,3}&l_{5,4}&l_{5,5}\end{pmatrix}.$$

For definiteness, we assume $\lambda_1<0$ and $\lambda_5>\lambda_2=\lambda_3=\lambda_4>0$. Thus one boundary condition is needed at P_0. For example, the normal momentum is prescribed $\widehat{U}_2(\boldsymbol{x}_0,t)=g_2(t)$.

The local characteristic variables V_m at grid points near P_0 are defined by

$$(V_m)_{\mu,\nu}=\boldsymbol{l}_m\left(\widehat{\boldsymbol{U}}_0\right)\widehat{\boldsymbol{U}}_{\mu,\nu},\quad m=1,\dots,5,\quad (x_\mu,y_\nu)\in\mathcal{E}_{i,j},\tag{2.18}$$

where $\mathcal{E}_{i,j}\subset\Omega$ is a set of grid points used for extrapolation. We extrapolate $(V_m)_{\mu,\nu}$ to P_0 and denote the extrapolated kth order $\hat{x}$-derivative of V_m by $V_m^{*(k)},\ k=0,\dots,4$. The choice of $\mathcal{E}_{i,j}$ and the fifth order WENO type extrapolation in 2D will be described in detail in the next subsection.

We solve $\widehat{U}_m^{*(0)}$ by a linear system of equations

$$\begin{pmatrix}0&1&0&0&0\\ l_{2,1}&l_{2,2}&l_{2,3}&l_{2,4}&l_{2,5}\\ l_{3,1}&l_{3,2}&l_{3,3}&l_{3,4}&l_{3,5}\\ l_{4,1}&l_{4,2}&l_{4,3}&l_{4,4}&l_{4,5}\\ l_{5,1}&l_{5,2}&l_{5,3}&l_{5,4}&l_{5,5}\end{pmatrix}\begin{pmatrix}\widehat{U}_1^{*(0)}\\ \widehat{U}_2^{*(0)}\\ \widehat{U}_3^{*(0)}\\ \widehat{U}_4^{*(0)}\\ \widehat{U}_5^{*(0)}\end{pmatrix}=\begin{pmatrix}g_2(t_n)\\ V_2^{*(0)}\\ V_3^{*(0)}\\ V_4^{*(0)}\\ V_5^{*(0)}\end{pmatrix}.\tag{2.19}$$

Here the first equation is the prescribed boundary condition. The other equations represent extrapolation of the four outgoing characteristic variables V_m, $m=2,\dots,5$. Next, we use the ILW procedure for $\widehat{U}_2$. The second equation of (2.16) gives us

$$\frac{\partial\widehat{U}_2}{\partial t}=-\left(\frac{\gamma-3}{2}\frac{\widehat{U}_2^2}{\widehat{U}_1^2}+\frac{\gamma-1}{2}\frac{\widehat{U}_3^2}{\widehat{U}_1^2}\right)\frac{\partial\widehat{U}_1}{\partial\hat{x}}-(3-\gamma)\frac{\widehat{U}_2}{\widehat{U}_1}\frac{\partial\widehat{U}_2}{\partial\hat{x}}+(\gamma-1)\frac{\widehat{U}_3}{\widehat{U}_1}\frac{\partial\widehat{U}_3}{\partial\hat{x}}-(\gamma-1)\frac{\partial\widehat{U}_4}{\partial\hat{x}}+Q(\gamma-1)\frac{\partial\widehat{U}_5}{\partial\hat{x}}-\frac{\partial}{\partial\hat{y}}\left(\frac{\widehat{U}_2\widehat{U}_3}{\widehat{U}_1}\right).$$

At the boundary, the left-hand side of the above equation is the known function $g_2'(t)$. The tangential derivative on the right-hand side can be computed by numerical differentiation, since we have obtained $\widehat{U}_m^{*(0)}$ of all the ghost points. Thus $\widehat{U}_m^{*(1)}$ can be solved by the linear system

$$\boldsymbol{A}^{*(0)}\begin{pmatrix}\widehat{U}_1^{*(1)}\\ \widehat{U}_2^{*(1)}\\ \widehat{U}_3^{*(1)}\\ \widehat{U}_4^{*(1)}\\ \widehat{U}_5^{*(1)}\end{pmatrix}=\begin{pmatrix}-g_2'(t_n)-\frac{\partial}{\partial\hat{y}}\left(\frac{\widehat{U}_2^{*(0)}\widehat{U}_3^{*(0)}}{\widehat{U}_1^{*(0)}}\right)\\ V_2^{*(1)}\\ V_3^{*(1)}\\ V_4^{*(1)}\\ V_5^{*(1)}\end{pmatrix},\tag{2.20}$$

where

$$\boldsymbol{A}^{*(0)}=\begin{pmatrix}\frac{\gamma-3}{2}\left(\frac{\widehat{U}_2^{*(0)}}{\widehat{U}_1^{*(0)}}\right)^2+\frac{\gamma-1}{2}\left(\frac{\widehat{U}_3^{*(0)}}{\widehat{U}_1^{*(0)}}\right)^2&(3-\gamma)\frac{\widehat{U}_2^{*(0)}}{\widehat{U}_1^{*(0)}}&(1-\gamma)\frac{\widehat{U}_3^{*(0)}}{\widehat{U}_1^{*(0)}}&\gamma-1&Q(1-\gamma)\\ l_{2,1}&l_{2,2}&l_{2,3}&l_{2,4}&l_{2,5}\\ l_{3,1}&l_{3,2}&l_{3,3}&l_{3,4}&l_{3,5}\\ l_{4,1}&l_{4,2}&l_{4,3}&l_{4,4}&l_{4,5}\\ l_{5,1}&l_{5,2}&l_{5,3}&l_{5,4}&l_{5,5}\end{pmatrix}.$$

Repeatedly using Eq. (2.16) and the extrapolation equations, we are able to solve $\widehat{U}_m^{*(k)},\ k=2,3,4$. However, the algebra of the ILW procedure becomes extremely complicated for Eq. (2.16), which makes the implementation impractical. As for 1D problems, we can avoid the cumbersome ILW and use extrapolation only. $\widehat{U}_m^{*(k)},\ k=2,3,4$, can be solved by

$$\boldsymbol{L}\left(\widehat{\boldsymbol{U}}_0\right)\begin{pmatrix}\widehat{U}_1^{*(k)}\\ \widehat{U}_2^{*(k)}\\ \widehat{U}_3^{*(k)}\\ \widehat{U}_4^{*(k)}\\ \widehat{U}_5^{*(k)}\end{pmatrix}=\begin{pmatrix}V_1^{*(k)}\\ V_2^{*(k)}\\ V_3^{*(k)}\\ V_4^{*(k)}\\ V_5^{*(k)}\end{pmatrix}. \tag{2.21}$$

An important class of boundary conditions for (reactive) Euler equations is the no-penetration boundary condition at solid walls, i.e., $\hat{u}=0$ or $\widehat{U}_2=0$. In this case, the eigenvalues $\lambda_1\approx -c_0<0$, $\lambda_5\approx c_0>0$ and $\lambda_2=\lambda_3=\lambda_4\approx 0$. Since only one boundary condition is prescribed, we consider V_m, $m=2,\ldots,5$, to be outgoing and V_1 to be ingoing, which falls into the same case as discussed above. (2.19) gives us $\widehat{U}_2^{*(0)}=0$. Then the first equation of (2.20) reduces to

$$\frac{\gamma-1}{2}\left(\frac{\widehat{U}_3^{*(0)}}{\widehat{U}_1^{*(0)}}\right)^2\widehat{U}_1^{*(1)}+(1-\gamma)\frac{\widehat{U}_3^{*(0)}}{\widehat{U}_1^{*(0)}}\widehat{U}_3^{*(1)}+(\gamma-1)\widehat{U}_4^{*(1)}-Q(\gamma-1)\widehat{U}_5^{*(1)}=\frac{\left(\widehat{U}_3^{*(0)}\right)^2}{R\widehat{U}_1^{*(0)}}, \tag{2.22}$$

where R is the radius of curvature of $\partial\Omega$ at P_0. Notice that there is no tangential derivative in (2.22). Therefore, we do not need to do any numerical differentiation, which further simplifies the implementation.

(2.22) can also be derived by considering primitive variables, i.e., $\rho,\ \hat{u},\ \hat{v},\ p$ and Y, in the ILW procedure. At the solid walls, we obtain

$$\frac{\partial p}{\partial\hat{x}}=\rho\frac{\hat{v}^2}{R}, \tag{2.23}$$

which is equivalent to (2.22) because of the equation of state (2.14). In fact, it is sometimes more convenient to use primitive variables than to use conservative variables $\boldsymbol{U}$. The performance of the former is good as illustrated in [21].

We now summarize our fifth order boundary treatment for the 2D problem (2.13). We assume the values of all the grid points inside Ω have been updated from time level t_{n-1} to time level t_n. Our goal is to impose the value of $\left(\widehat{U}_m\right)_{i,j},\ m=1,\ldots,5$, for each ghost point (x_i,y_j).

1. For each ghost point (x_i,y_j), we do the following three steps:
   - Decide the local coordinate system (2.15). Compute the eigenvalues $\lambda_m\left(\widehat{\boldsymbol{U}}_0\right)$ and left eigenvectors $\boldsymbol{l}_m\left(\widehat{\boldsymbol{U}}_0\right)$ of the Jacobian matrix $\boldsymbol{A}_\perp\left(\widehat{\boldsymbol{U}}_0\right)$ for $m=1,\ldots,5$. Decide the prescribed inflow boundary conditions $g_m(t)$ according to the signs of $\lambda_m\left(\widehat{\boldsymbol{U}}_0\right)$.
   - Form the local characteristic variables $(V_m)_{\mu,\nu},\ (x_\mu,y_\nu)\in\mathcal{E}_{i,j}$, as in (2.18). Extrapolate $(V_m)_{\mu,\nu}$ to the boundary to obtain $V_m^{*(k)},\ k=0,\ldots,4$, with fifth order WENO type extrapolation. Details of the 2D extrapolation will be discussed in the next subsection.
   - Solve for $\widehat{U}_m^{*(0)},\ m=1,\ldots,5$, by the prescribed boundary conditions and extrapolated values $V_m^{*(0)}$, such as (2.19).
2. For each ghost point (x_i,y_j), use the ILW procedure to write the first derivative of $g_m(t)$ as a linear combination of first normal derivatives plus tangential derivatives. Together with the extrapolation equations, form a linear system with $\widehat{U}_m^{*(1)}$ as unknowns, such as (2.20). Solve for $\widehat{U}_m^{*(1)},\ m=1,\ldots,5$. For $k=2,3,4$, solve for $\widehat{U}_m^{*(k)}$ by extrapolation equations (2.21) where the ILW procedure is not needed.
3. Impose the values of the ghost points by the Taylor expansion (2.17).

If no-penetration boundary condition is considered at solid walls, then the first equation of (2.20) is replaced by (2.22) in Step 2 with other steps unchanged. An alternative is to use primitive variables instead of conservative variables.

2.4. 2D WENO type extrapolation

We return to the issue of 2D fifth order WENO type extrapolation. It is needed in the second bullet of Step 1 of the algorithm flowchart in Section 2.3, regardless of the smoothness of the solution. For stability reason, we used third order least squares extrapolation if the solution is smooth near the boundary or third order WENO type extrapolation otherwise in [20]. Our fifth order extrapolation should combine the features of both. Namely, more points are needed to construct a 2D extrapolating polynomial and the extrapolation should not have severe overshoot or undershoot near the discontinuities.

For a given ghost point (x_i,y_j), we aim to first construct a stencil $\mathcal{E}\subset\Omega$ for extrapolation and then to obtain a $(5-k)$th order approximation of $\left.\frac{\partial^k V}{\partial\hat{x}^k}\right|_{(x,y)=\boldsymbol{x}_0}$, which is denoted by $V^{*(k)},\ k=0,\ldots,4$. Compared with the notations used in Section

2.3, here we suppress the subscripts indicating the mth component of V and that the stencil $\mathcal{E}$ is for the ghost point (x_i, y_j). $\mathcal{E} = \bigcup_{r=0}^{4} \mathcal{E}_r$ consists of five substencils $\mathcal{E}_r,\ r = 0, \ldots, 4$, each of which is for constructing a least squares polynomial $p_r(x,y)$ in P^r, i.e.,

$$p_r(x,y) = \sum_{0 \leqslant m+l \leqslant r} a_{lm} x^l y^m,$$

satisfying

$$p_r(x_\mu, y_\nu) = V_{\mu,\nu}, \quad \text{for all } (x_\mu, y_\nu) \in \mathcal{E}_r. \tag{2.24}$$

Notice that $p_r(x,y)$ has $(r+1)(r+2)/2$ degrees of freedom. We choose $\mathcal{E}_r$ such that it contains $(r+1)^2$ points and (2.24) holds in the sense of least squares if $r > 0$.

We take $r = 3$ as an example to show how to choose $\mathcal{E}_r$. $\mathcal{E}_3$ is composed of 16 square points sketched in Fig. 2.1. It contains four 1D substencils $\mathcal{S}_l,\ l = 0, \ldots, 3$. Suppose the normal $\boldsymbol{n}(x_0)$ (or $\hat{x}$-axis) intersects the grid line $y = y_{n-l}$ at a point P_l^*. We denote the grid point on the horizontal line $y = y_{n-l}$ which is just to the left of P_l^* by (x_m^l, y_{n-l}). Then we set

$$\mathcal{S}_l = \left\{ (x_{m-1}^l, y_{n-l}), (x_m^l, y_{n-l}), (x_{m+1}^l, y_{n-l}), (x_{m+2}^l, y_{n-l}) \right\}, \quad l = 0, \ldots, 3,$$

and $\mathcal{E}_3 = \bigcup_{l=0}^{3} \mathcal{S}_l$. Notice that we have to shift $\mathcal{S}_0$ to the left by one grid point so that $\mathcal{S}_0$ lies in Ω.

On each $\mathcal{E}_r,\ r = 0, \ldots, 4,\ V^{*(k)}$ can be extrapolated by

$$V^{*(k)} = \frac{\partial^k}{\partial \hat{x}^k} p_r(x,y) \bigg|_{(x,y)=\boldsymbol{x}_0}.$$

We seek WENO type extrapolation of the form

$$V^{*(k)} = \sum_{r=0}^{4} \omega_r \frac{\partial^k}{\partial \hat{x}^k} p_r(x,y) \bigg|_{(x,y)=\boldsymbol{x}_0}, \tag{2.25}$$

where ω_r are nonlinear weights. The nonlinear weights ω_r are defined by

$$\omega_r = \frac{\alpha_r}{\sum_{s=0}^{4} \alpha_s}$$

with

$$\alpha_r = \frac{d_r}{(\varepsilon + \beta_r)^q}, \tag{2.26}$$

where $d_0 = 2h^4,\ d_1 = 2h^3,\ d_2 = 2h^2,\ d_3 = 2h,\ d_4 = 1 - \sum_{r=0}^{3} d_r,\ \varepsilon = 10^{-6}$ and $q \geqslant 3$ is an integer. The smoothness indicators β_r are determined by

$$\beta_0 = 2h^2,$$
$$\beta_r = \sum_{1 \leqslant |\alpha| \leqslant r} \int_K |K|^{|\alpha|-1} (D^\alpha p_r(x,y))^2 \, dx\, dy, \quad r = 1, \ldots, 4,$$

where α is a multi-index and $K = [x_0 - h/2, x_0 + h/2] \times [y_0 - h/2, y_0 + h/2]$. We can show that (2.25) is $(5-k)$th order accurate if V is smooth in $\mathcal{E}$ and ω_r vanishes as $h \to 0$ if $\mathcal{E}_r$ contains a discontinuity.

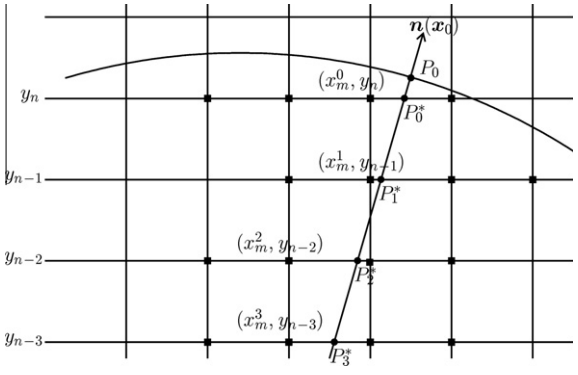

Fig. 2.1. The choice of $\mathcal{E}_3$ (square points) for 2D WENO type extrapolation.

Notice that the stencil $\mathcal{E}$ for the fifth order WENO type extrapolation contains at least 25 grid points. For most cases, it is eventually possible to fit the wide stencil in the computational domain by mesh refinement. However, in some special cases, we have to reduce the order of extrapolation. See, for example, Example 5 in [21].

3. Numerical examples

We test our fifth order boundary treatment in this section. For accuracy tests, we take $\Delta t = O(h^{5/3})$ in the third order RK time integration (2.3) in order to have fifth order accuracy in time. For other cases, we take $\Delta t = O(h)$ and the CFL number as 0.6. The specific heat ratio γ in (reactive) Euler equations is taken as $\gamma = 1.4$ and the power q in (2.12) or (2.26) is taken as $q = 3$, unless otherwise indicated. The L^1 error and L^∞ error are defined as $h^2\sum_{\{(i,j):(x_i,y_j)\in\mathcal{D}\}}|e_{i,j}|$ and $\max_{\{(i,j):(x_i,y_j)\in\mathcal{D}\}}|e_{i,j}|$, respectively. Here $e_{i,j}$ denotes the error at grid point (x_i,y_j) and $\mathcal{D}$ is the region where the errors are measured. $\mathcal{D} = \Omega$ unless otherwise indicated.

3.1. 1D Euler equations

Example 1. We redo Example 3(a) in [20] with the simplified and improved algorithm. The domain is $(-\pi,\pi)$ and the initial condition is

$$\rho(x,0) = 1 + 0.2\sin x,$$
$$u(x,0) = 1,$$
$$p(x,0) = 2.$$

We want to impose the boundary conditions such that the exact solution is simply a translation of the initial condition

$$p(x,t) = 1 + 0.2\sin(x-t),$$
$$u(x,t) = 1,$$
$$p(x,t) = 2.$$

At both boundaries, we have $\lambda_1 < 0$ and $\lambda_3 > \lambda_2 > 0$. We prescribe $\rho(-\pi,t)$, $u(-\pi,t)$ and $\rho(\pi,t)$. The density errors are listed in Table 3.1. We can clearly see the designed fifth order convergence.

Example 2. We consider the interaction of two blast waves [26]. The initial data are

$$\boldsymbol{U}(x,0) = \begin{cases} \boldsymbol{U}_L & 0 < x < 0.1, \\ \boldsymbol{U}_M & 0.1 < x < 0.9, \\ \boldsymbol{U}_R & 0.9 < x < 1, \end{cases}$$

where $\rho_L = \rho_M = \rho_R = 1$, $u_L = u_M = u_R = 0$, $p_L = 10^3$, $p_M = 10^{-2}$, $p_R = 10^2$. There are solid walls at both $x = 0$ and $x = 1$. This problem involves multiple reflections of shocks and rarefactions off the walls. The density profile at $t = 0.038$ is shown in Fig. 3.1(a) with $h = 1/800$ and in Fig. 3.1(b) with $h = 1/1600$. The reference solution is computed by the fifth order WENO scheme with $h = 1/16000$, together with the reflection technique at both boundaries. Our fifth order boundary treatment gives an excellent non-oscillatory resolution. The results are similar to those obtained by a third order boundary treatment in Example 4 of [20].

3.2. 2D Euler equations

Example 3. We test the vortex evolution problem on a disk $\Omega = \{(x,y): x^2 + y^2 < 0.5\}$. The mean flow is $\rho = p = u = v = 1$. We add to this mean flow an isentropic vortex perturbation centered at $(x_0,y_0) = (0.3,0.3)$ in (u,v) and in the temperature $T = p/\rho$, no perturbation in the entropy $S = p/\rho^\gamma$

Table 3.1
Density errors and convergence rates of Example 1, $h = 2\pi/N$, $t = 2$.

N	L^1 error	Order	L^∞ error	Order
40	7.02E−05		5.84E−04	
80	2.82E−07	7.96	2.84E−06	7.69
160	3.16E−09	6.48	1.78E−08	7.31
320	9.89E−11	5.00	5.58E−10	5.00
640	3.06E−12	5.02	1.73E−11	5.01

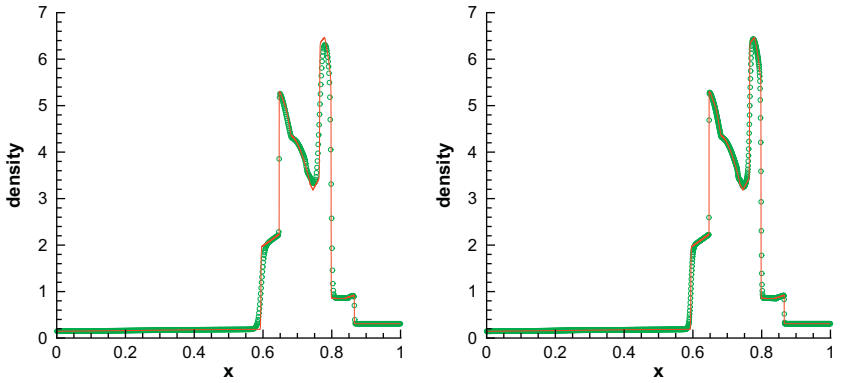

(a) $h = 1/800$ (b) $h = 1/1600$

Fig. 3.1. The density profiles of the blast wave problem. Solid lines: reference solution computed by the fifth order WENO scheme with $h = 1/16000$, together with the reflection technique at boundaries; symbols: numerical solutions by our fifth order boundary treatment.

$$(\delta u, \delta v) = \frac{\epsilon}{2\pi} e^{0.5(1-r^2)}(-\bar{y}, \bar{x}),$$
$$\delta T = -\frac{(\gamma-1)\epsilon^2}{8\gamma\pi^2} e^{(1-r^2)},$$
$$\delta S = 0,$$

where $(\bar{x}, \bar{y}) = (x - x_0, y - y_0)$, $r^2 = \bar{x}^2 + \bar{y}^2$ and the vortex strength is $\epsilon = 5$. We regard the exact solution $U(x,y,t)$ as the passive convection of the vortex with the mean velocity and take boundary conditions from $U(x,y,t)$ whenever needed. The number of boundary conditions is determined by the signs of the four eigenvalues λ_m which vary both in space and in time. This problem was tested by a third order boundary treatment in Example 7 of [20]. Here we are able to test our fifth order method, thanks to the simplified algorithm. The density errors are listed in Table 3.2. We can see that the designed fifth order convergence is achieved in the L^1 norm.

Table 3.2
Density errors of the vortex evolution problem on a disk, $t = 0.1$.

h	L^1 error	Order	L^∞ error	Order
1/20	1.94E−07		2.55E−05	
1/40	3.66E−09	5.73	1.94E−07	7.04
1/80	1.22E−10	4.91	1.07E−08	4.17
1/160	4.26E−12	4.83	6.00E−10	4.16

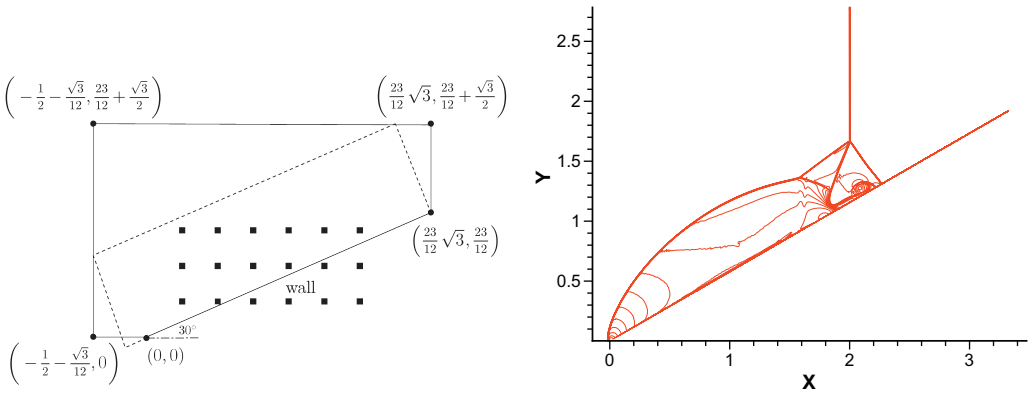

(a) computational domain (b) density contour

Fig. 3.2. Left: The computational domain (solid line) of the double Mach reflection problem. The dashed line indicates the computational domain used in [9,17]. The square points indicate some of the grid points near the wall. Illustrative graph, not to scale. Right: Density contour of double Mach reflection, 30 contour lines from 1.731 to 20.92. $h = 1/320$.

Example 4. We test the double Mach reflection problem [26] which involves a solid wall not aligned with the grid lines. This problem is initialized by sending a horizontally moving shock into a solid wall inclined by a 30° angle. In order to impose the no-penetration boundary condition by the reflection technique, people usually solve an equivalent problem that puts the wall horizontal and puts the shock 60° angle inclined to the wall, see for example [9,17]. We consider the solution of the equivalent problem as our reference solution.

We solve the original problem on a uniform mesh with our fifth order boundary treatment in conservative variables. The problem setup is the same as in Example 8 of [20]. The computational domain is sketched in Fig. 3.2(a), together with some of the grid points near the wall indicating that the wall is not aligned with the grid lines. Initially a right-moving Mach 10 shock is positioned at (0,0). At $y = 0$, the exact postshock condition is imposed. At the top boundary, the flow values are set to describe the exact motion of the Mach 10 shock. Supersonic inflow and outflow boundary conditions are used at the left and right boundary, respectively. The power q in (2.26) is taken as $q = 20$ to stabilize our boundary treatment. Fig. 3.2(b) shows the density contour with $h = 1/320$ at $t = 0.2$. A zoomed-in region near the double Mach stem is shown in Fig. 3.3(a). The region is rotated and translated for the ease of comparison. In Fig. 3.3(b), we show the reference solution on a mesh with comparable size. Fig. 3.3(c) and (d) show the density contours on a refined mesh. Compared with the results in [20], our results here seem to be closer to the reference solution in terms of the location of the "blown-up" portion around the double Mach stem.

Example 5. This is an example involving a curved wall. The problem is initialized by a Mach 3 flow moving toward a circular cylinder of unit radius positioned at the origin on a x–y plane. The problem setup is the same as in Example 9 of [20]. The computational domain is the upper half of the physical domain shown in Fig. 3.4(a), due to the symmetry of this problem. At $y = 0$, the reflection technique is used. Supersonic inflow boundary condition is used at the left boundary $x = -3$; supersonic outflow boundary condition is used at the top boundary $y = 6$ and at the right boundary $x = 0$. Our fifth order boundary treatment in primitive variables with $q = 10$ in (2.26) is applied at the surface of the cylinder. Notice that although the initial condition is incompatible with the no-penetration boundary condition, we do not encounter any problem if using primitive variables, while difficulty arises if we use conservative variables as reported in [20].

The pressure contour at steady state is shown in Fig. 3.4(b) and (c) with different mesh sizes. The bow shock is well-captured by our method. For a more quantitative verification, we take advantage of the entropy along the surface, which can be computed analytically by using the Rankine–Hugoniot conditions for the streamline normal to the bow shock at $y = 0$. Since there is usually no grid point located on the surface, we compute the entropy errors of the state $\widehat{U}_m^{*(0)}$, $m = 1, \ldots, 4$, which is the constant term in the Taylor expansion (2.17), for all the ghost points. We can see superlinear convergence rates in Table 3.3. In other words, although the accuracy of our high order boundary treatment degenerates to first order near the shock, it is expected to be higher than first order in the smooth part of the solution.

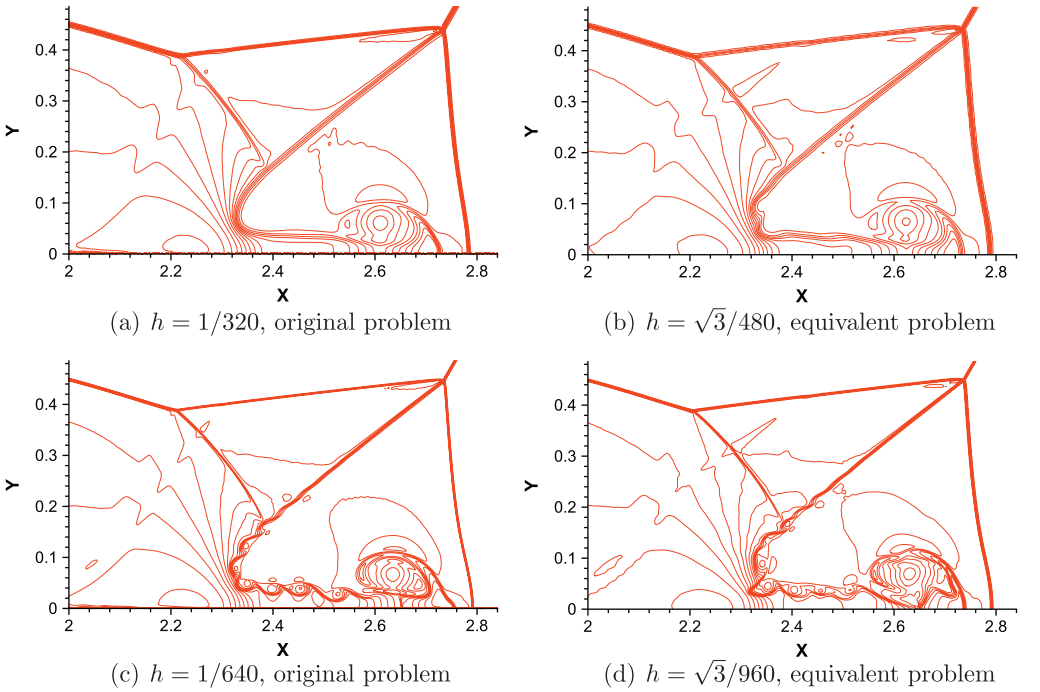

Fig. 3.3. Density contours of double Mach reflection, 30 contour lines from 1.731 to 20.92. Zoomed-in near the double Mach stem. The plots in the left column are rotated and translated for comparison.

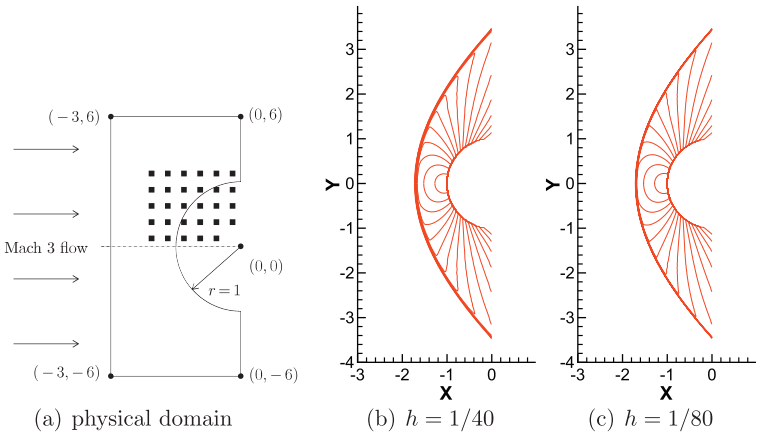

(a) physical domain (b) $h = 1/40$ (c) $h = 1/80$

Fig. 3.4. Left: physical domain of flow past a cylinder. The computational domain is the upper half. The square points indicate some of the grid points near the cylinder. Illustrative sketch, not to scale. Others: pressure contours of flow past a cylinder, 20 contour lines from 2 to 15.

Table 3.3
L^∞ entropy errors on the surface of the cylinder and rates of convergence of Example 5.

h	L^∞ error	Order
1/20	1.68E−02	
1/40	7.06E−03	1.25
1/80	1.88E−03	1.91
1/160	7.50E−04	1.33

3.3. 2D reactive Euler equations

Example 6. We would like to test the accuracy of our boundary treatment for 2D reactive Euler equations in this example. Unfortunately, it is difficult to construct an analytical solution with no-penetration boundary condition at solid curved walls. We follow the idea in Example 4 of [21] to construct isentropic flows so that we are able to measure the entropy errors. We set the source term $\omega = 0$ in (2.13) such that isentropic flows can be maintained as long as the flows keep smooth. Namely, we only consider the transport of the chemical reactants. The heat release is set to $Q = 2$.

We consider a region $[-4,4] \times [-4,4]$ with all the boundaries as solid walls. A circular cylinder with unit radius is centered at the origin. The computational domain is then $\Omega = [-4,4] \times [-4,4] \cap \{(x,y): x^2 + y^2 > 1\}$. The initial conditions should be compatible with the no-penetration boundary condition at the solid walls and at the surface of the cylinder. For this purpose, we set

$$u(x,y,0) = \lambda_1(x,y)u_1(x,y),$$
$$v(x,y,0) = \frac{1}{2}[\lambda_1(x,y)v_1(x,y) + \lambda_2(x,y)v_2(x,y)],$$

where

$$\lambda_1(x,y) = \frac{\left(4\sqrt{2}-1\right)\left(\sqrt{x^2+y^2}-1\right)}{\left(\sqrt{16+y^2}-1\right)\left(\sqrt{16+x^2}-1\right)},$$
$$\lambda_2(x,y) = \frac{\sqrt{x^2+y^2}(x^2-16)(y^2-16)}{\left(\frac{x^2}{x^2+y^2}-16\right)\left(\frac{y^2}{x^2+y^2}-16\right)},$$
$$u_1(x,y) = \sin\left(\frac{\pi}{4}x\right)\sin^2\left(\frac{\pi}{4}y\right),$$
$$v_1(x,y) = u_1(y,x),$$
$$v_2(x,y) = \frac{1}{16}(x^2+y^2-1)\sin\left(\frac{\pi}{4}x\right).$$

The other initial conditions are $\rho(x,y,0) = p(x,y,0) = 1$ and

$$Y(x,y,0) = \frac{1}{2}\left[1 + \sin^2\left(\frac{\pi}{4}x\right)\sin^2\left(\frac{\pi}{4}y\right)\right].$$

We apply our fifth order boundary treatment in primitive variables at the surface of the cylinder and the reflection technique at the solid walls. Fig. 3.5 shows the density contour with $h = 1/20$ at $t = 0.5$. The entropy errors in the region $[-3,3] \times [-3,3]$ at the same time level are listed in Table 3.4. Fifth order convergence is achieved.

Example 7. We start to consider problems involving detonations. It is a rapid regime of burning in which a strong shock ignites the combustible mixture of gases and the burning proceeds to equilibrium behind the shock, while the energy released continues to help to drive the shock [16]. The first problem is the reflection of detonation waves on a wedge, see [8,22] for experiments and [14,25] for numerical simulations. The computational domain is sketched in Fig. 3.6(a). A Zeldovich, von Neumann and Doering (ZND) profile with $T^+ = 50$, $Q = 50$, $f = 1.0$, $\gamma = 1.2$ is initially located at $x = -118.2$. Here f is the overdrive factor defined by $f = D^2/D_{CJ}^2$, where D is the detonation velocity and D_{CJ} is the velocity of the corresponding Chapman-Jouguet wave. The constant prestate is $(\rho, u, v, p, Y) = (1, 0, 0, 1, 1)$. See [2,28] for details about the ZND profile. The density and pressure fields of this profile are perturbed so that the instability of the flow results in the development of triple points, whose trajectories form a cellular pattern [2,4,16]. The perturbation is in the region $[-117.0, -115.8] \times [0, 100]$ in which

$$\rho(x,y,0) = p(x,y,0) = \begin{cases} 1.8 & \text{if } y \in [20,40] \cup [60,80], \\ 0.2 & \text{otherwise.} \end{cases}$$

Supersonic inflow and outflow boundary conditions are used at $x = -120$ and at $x = 120$, respectively. The reflection technique is applied at $y = 0$ and at $y = 100$. Our fifth order boundary treatment in conservative variables with $q = 40$ in (2.26) is used at the surface of the wedge.

We first set the wedge angle $\theta = 19.3°$. We run the code until $t = 28$ with $h = 0.15$. Fig. 3.7(a) shows the cellular detonation pattern determined by recording the history of the maximum pressure. The cellular pattern is similar to the experimental results in Figs. 5, 10, 11 of [8] and the numerical results in Fig. 8 of [25]. From Fig. 3.7(a), we can observe the main feature of

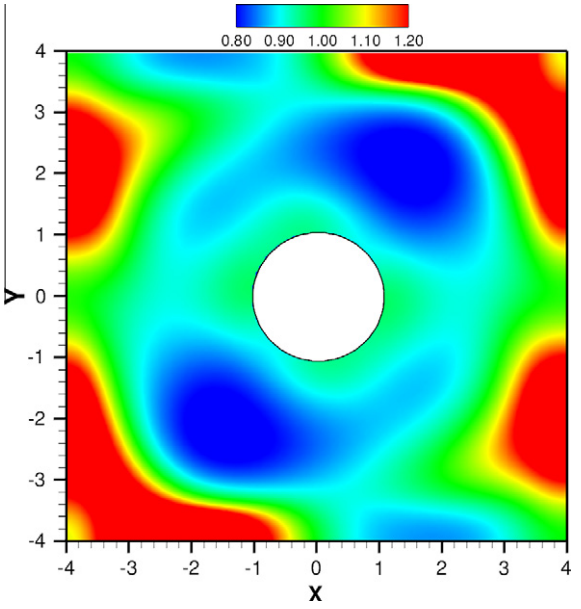

Fig. 3.5. Density contour of Example 6, $h = 1/20$, $t = 0.5$.

Table 3.4
Entropy errors in $[-3,3] \times [-3,3]$ and convergence rates of Example 6, $t = 0.5$.

h	L^1 error	Order	L^∞ error	Order
1/5	1.44E−03		5.67E−04	
1/10	5.00E−05	4.84	2.72E−05	4.38
1/20	8.66E−07	5.85	5.03E−07	5.76
1/40	2.26E−08	5.26	1.81E−08	4.80

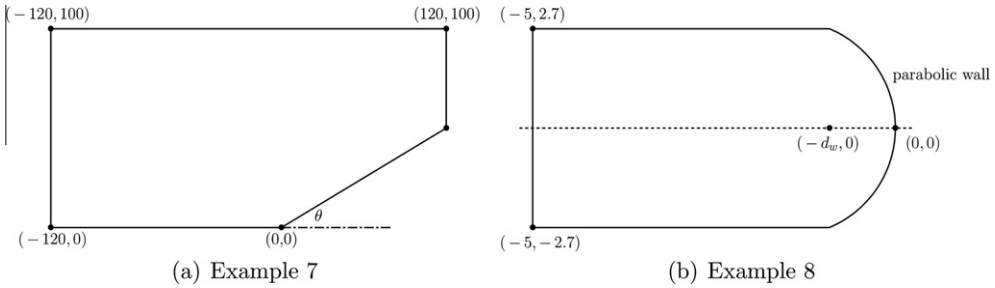

Fig. 3.6. Left: computational domain of Example 7. Right: physical domain of Example 8. The computational domain is the upper half. Both are illustrative sketches, not to scale.

the detonation wave reflection. There is a sharp dividing line, made up by a triple point trajectory, emerging near the tip of the wedge and extending downstream. The detonation cells below the line are smaller than those above the line and are distorted in shape.

Next, we increase the wedge angle to $\theta = 30^\circ$ and keep other parameters unchanged. The cellular pattern at $t = 30$ with $h = 0.15$ is shown in Fig. 3.7(b). As the experimental results in Fig. 1(d) of [22], Fig. 7 of [8] and the numerical result in Fig. 9 of [14], the cellular pattern is not clear in this case since the spatial scale of the region between the wedge and the reflection of transverse waves is small. However, the dividing line is still quite sharp.

Example 8. We consider the shock focusing problem. The physical domain is sketched in Fig. 3.6(b). The curve represents a solid wall with parabolic shape. A right-moving Mach 2.5 shock is initially positioned at $x = -d_w$, where d_w is the depth of the parabolic wall. The preshock state is $(\rho, u, v, p, Y) = (0.2, 0, 0, 0.2, 1)$. As the incident shock wave enters the cavity of the end-wall, there are local zones with elevated pressure and temperature. The formation of such hot zones causes self-ignition which is sometimes followed by detonation initiation. See [5] for experiments and [1] for numerical simulations.

We set $T^+ = 20$, $Q = 50$ and $K_c = 30$. The computational domain is the upper half of the physical domain due to the symmetry of this problem. The reflection technique is used at $y = 0$ and at $y = 2.7$. Supersonic inflow boundary condition is used at the left boundary $x = -5$. Our fifth order boundary treatment in primitive variables with $q = 40$ in (2.26) is applied at the parabolic wall.

In the first case, we consider a parabola $y^2 = -2.7x$ with $d_w = 2.7$. The temperature contours with $h = 1/160$ and $h = 1/320$ at different times are shown in Fig. 3.8. At $t = 0.8$, a high temperature ignition zone is formed at the lateral surface near the Mach stem (see the top row of Fig. 3.8), which shows that focusing induces exothermic reaction of combustible gases. The primary ignition starts and the developing detonation waves are focused around the center line (see the middle row). Similar structure persists until the detonation leaves the cavity of the end-wall (see the bottom row).

In the second case, we consider a shorter parabola $y^2 = -4.5x$ with $d_w = 1.62$. Other parameters are kept the same. The temperature contours with $h = 1/160$ and $h = 1/320$ at different times are shown in Fig. 3.9. We again obtain convergent solutions with good resolutions.

4. Concluding remarks

We improve the high order numerical boundary condition developed in [20] in two aspects. First, we find that the ILW procedure is not needed for obtaining kth order normal derivative for $k \geqslant 2$, regardless of the direction of the local charac-

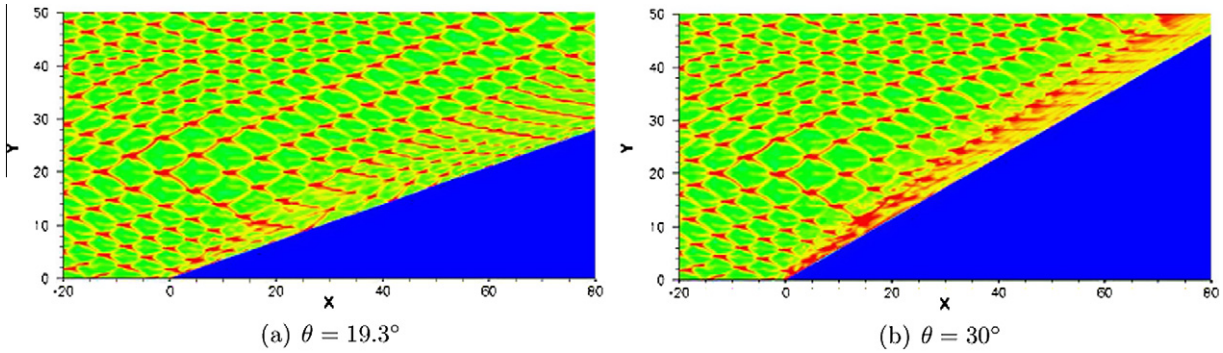

Fig. 3.7. Cellular patterns of detonation waves over a wedge of angle θ.

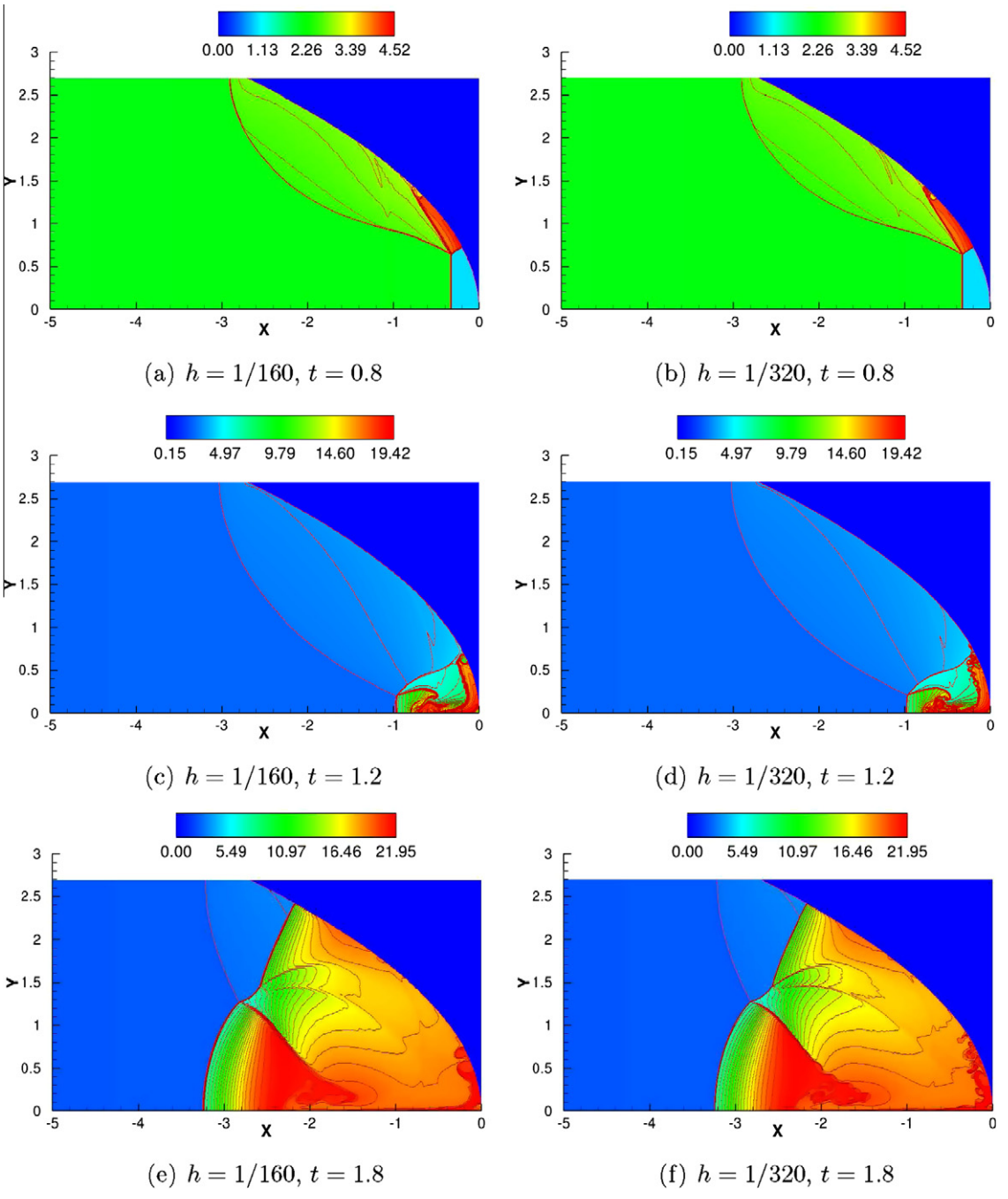

Fig. 3.8. Temperature contours of the shock focusing problem. 29 Contour lines in the respective range. $d_w = 2.7$. The color outside the computational domain is not relevant. (For interpretation of the references to colour in this figure legend, the reader is referred to the web version of this article.)

teristics. This makes the implementation of fifth order boundary treatment practical for 2D nonlinear systems with source terms. For no-penetration boundary condition at solid walls, the tangential derivative terms involved in the ILW procedure can be avoided to further simplify the implementation. Secondly, a fifth order WENO type extrapolation is designed such that our algorithm keeps the same for solutions with or without discontinuities. Various numerical examples, with or without chemical reactions, demonstrate that our improved boundary treatment is fifth order accurate and performs well even if there are complicated interactions between detonation/shock waves and solid boundaries. In future work, we will try to extend this boundary treatment to high order discontinuous Galerkin methods for compressible inviscid flows involving complex geometries on rectangular meshes.

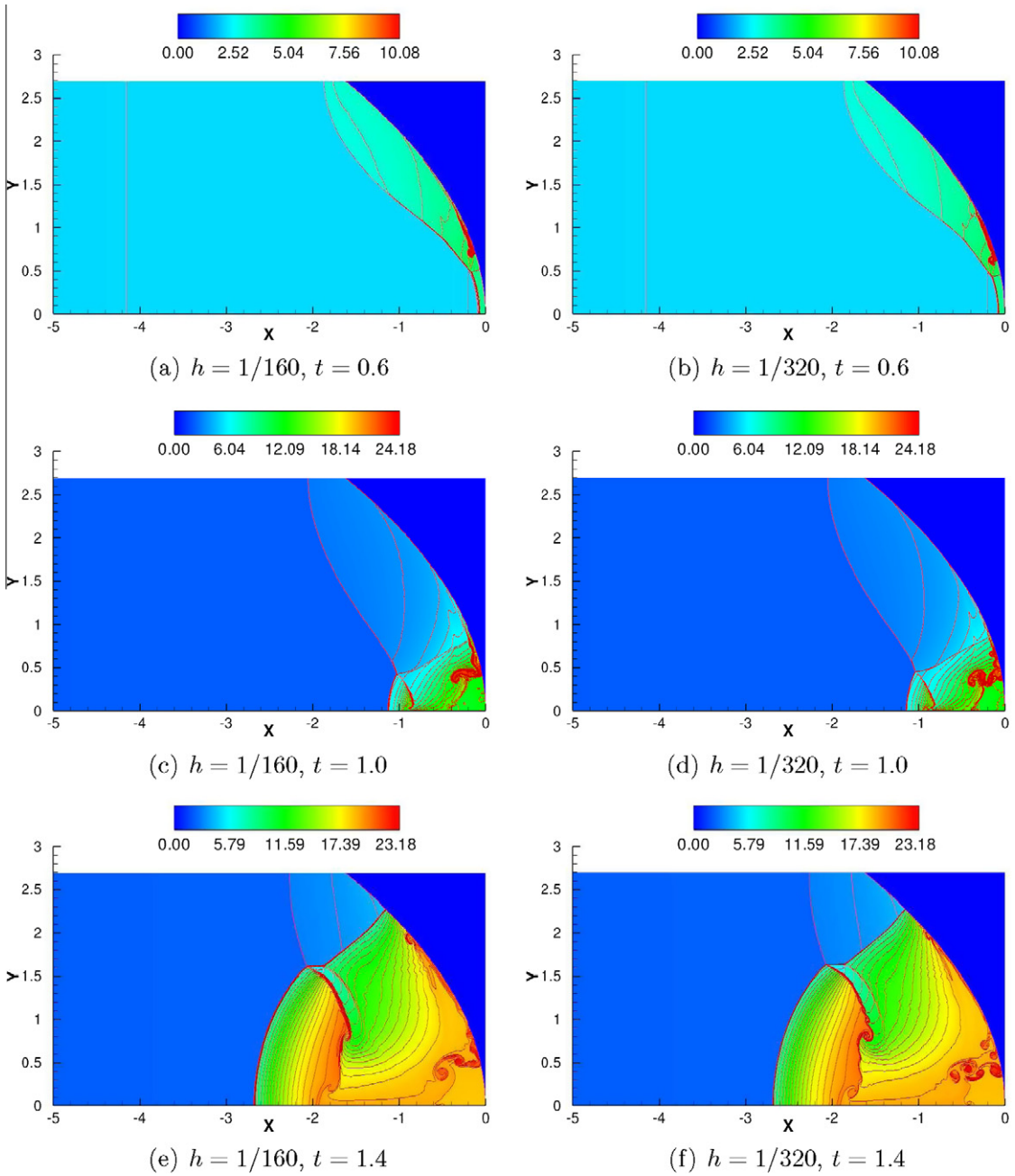

Fig. 3.9. Temperature contours of the shock focusing problem. 29 Contour lines in the respective range. $d_w = 1.62$. The color outside the computational domain is not relevant. (For interpretation of the references to colour in this figure legend, the reader is referred to the web version of this article.)

Acknowledgments

The research of S. Tan and C.-W. Shu is supported by AFOSR Grant FA9550-09-1-0126 and NSF Grant DMS-1112700. The research of C. Wang is supported by New Century Excellent Talents in University under Grant No. NCET-08-0043, NSFC Grant 10972040 and the Foundation of State Key Laboratory of Explosion Science and Technology (Grant No. ZDKT11-01). The research of J. Ning is supported by NSFC Grant 11032002.

References

[1] A.M. Bartenev, S.V. Khomik, B.E. Gelfand, H. Grönig, H. Olivier, Effect of reflection type on detonation initiation at shock-wave focusing, Shock Waves 10 (2000) 205–215.

[2] A. Bourlioux, A.J. Majda, Theoretical and numerical structure of unstable detonations, Philosophical Transactions of the Royal Society of London A 350 (1995) 29–68.
[3] M.H. Carpenter, D. Gottlieb, S. Abarbanel, W.-S. Don, The theoretical accuracy of Runge–Kutta time discretizations for the initial boundary value problem: a study of the boundary error, SIAM Journal on Scientific Computing 16 (1995) 1241–1252.
[4] V.N. Gamezo, D. Desbordes, E.S. Oran, Two-dimensional reactive flow dynamics in cellular detonation waves, Shock Waves 9 (1999) 11–17.
[5] B.E. Gelfand, S.V. Khomik, A.M. Bartenev, S.P. Medvedev, H. Grönig, H. Olivier, Detonation and deflagration initiation at the focusing of shock waves in combustible gaseous mixture, Shock Waves 10 (2000) 197–204.
[6] M. Goldberg, E. Tadmor, Scheme-independent stability criteria for difference approximations of hyperbolic initial-boundary value problems. I, Mathematics of Computation 32 (1978) 1097–1107.
[7] M. Goldberg, E. Tadmor, Scheme-independent stability criteria for difference approximations of hyperbolic initial-boundary value problems. II, Mathematics of Computation 36 (1981) 603–626.
[8] C. Guo, D. Zhang, W. Xie, The Mach reflection of a detonation based on soot track measurements, Combustion and Flame 127 (2001) 2051–2058.
[9] G.-S. Jiang, C.-W. Shu, Efficient implementation of weighted ENO schemes, Journal of Computational Physics 126 (1996) 202–228.
[10] H.-O. Kreiss, N.A. Petersson, A second order accurate embedded boundary method for the wave equation with Dirichlet data, SIAM Journal on Scientific Computing 27 (2006) 1141–1167.
[11] H.-O. Kreiss, N.A. Petersson, J. Yström, Difference approximations for the second order wave equation, SIAM Journal on Numerical Analysis 40 (2002) 1940–1967.
[12] H.-O. Kreiss, N.A. Petersson, J. Yström, Difference approximations of the Neumann problem for the second order wave equation, SIAM Journal on Numerical Analysis 42 (2004) 1292–1323.
[13] J.-G. Ning, L.-W. Chen, Fuzzy interface treatment in Eulerian method, Science in China Series G: Physics, Mechanics & Astronomy 47 (2004) 550–568.
[14] S. Ohyagi, T. Obara, F. Nakata, S. Hoshi, A numerical simulation of reflection processes of a detonation wave on a wedge, Shock Waves 10 (2000) 185–190.
[15] J. Qiu, C.-W. Shu, Finite difference WENO schemes with Lax–Wendroff-type time discretizations, SIAM Journal on Scientific Computing 24 (2003) 2185–2198.
[16] G.J. Sharpe, S.A.E.G. Falle, Two-dimensional numerical simulations of idealized detonations, Philosophical Transactions of the Royal Society of London A 456 (2000) 2081–2100.
[17] J. Shi, Y.-T. Zhang, C.-W. Shu, Resolution of high order WENO schemes for complicated flow structures, Journal of Computational Physics 186 (2003) 690–696.
[18] C.-W. Shu, S. Osher, Efficient implementation of essentially non-oscillatory shock-capturing schemes, Journal of Computational Physics 77 (1988) 439–471.
[19] B. Sjögreen, N.A. Petersson, A Cartesian embedded boundary method for hyperbolic conservation laws, Communications in Computational Physics 2 (2007) 1199–1219.
[20] S. Tan, C.-W. Shu, Inverse Lax–Wendroff procedure for numerical boundary conditions of conservation laws, Journal of Computational Physics 229 (2010) 8144–8166.
[21] S. Tan, C.-W. Shu, A high order moving boundary treatment for compressible inviscid flows, Journal of Computational Physics 230 (2011) 6023–6036.
[22] G.O. Thomas, R.Ll. Williams, Detonation interaction with wedges and bends, Shock Waves 11 (2002) 481–492.
[23] C. Wang, T.-B. Ma, J. Lu, Influence of obstacle disturbance in a duct on explosion characteristics of coal gas, Science China: Physics, Mechanics and Astronomy 53 (2010) 269–278.
[24] C. Wang, T.-B. Ma, J.-G. Ning, Tracking method for multi-material interfaces and its application in shaped charge, Journal of Computational and Theoretical Nanoscience 5 (2008) 1512–1516.
[25] G. Wang, D. Zhang, K. Liu, J. Wang, An improved CE/SE scheme for numerical simulation of gaseous and two-phase detonations, Computers and Fluids 39 (2010) 168–177.
[26] P. Woodward, P. Colella, The numerical simulation of two-dimensional fluid flow with strong shocks, Journal of Computational Physics 54 (1984) 115–173.
[27] S. Xu, T. Aslam, D.S. Stewart, High resolution numerical simulation of ideal and non-ideal compressible reacting flows with embedded internal boundaries, Combustion Theory and Modelling 1 (1997) 113–142.
[28] Z.-C. Zhang, S.T.J. Yu, H. He, S.-C. Chang, Direct calculations of two- and three-dimensional detonations by an extended CE/SE method, AIAA Paper No. 2001-0476, 2001.